RESEARCH ARTICLE

Construction and performance evaluation of a plant polysaccharide hydrogel-based platform for simulating the detection of sweat glucose after exercise

Xiaoqin Xu*

Department of Physical Education, Hunan International Economics University, Changsha, Hunan, China.

Received: May 21, 2026. **Accepted:** September 29, 2026. **Published:** November 12, 2026.

Post-exercise sweat glucose can support non-invasive assessment of transient metabolic responses, but reliable monitoring is constrained by low glucose concentrations, variable sweat flow, and pH- and temperature-dependent signal drift. Existing platforms often optimize the sensing matrix, fluid handling, or readout separately. This *in vitro* study therefore constructed a plant polysaccharide hydrogel platform and compared eight formulations for controlled simulations of sweat glucose detection after exercise. The optimized alginate-pectin-carboxymethyl cellulose/cellulose nanocrystal/gold-Prussian blue (APC-CNC-AuPB) hydrogel was combined with enzymatic electrochemical and colorimetric readouts. Fourier transform infrared spectroscopy (FTIR), X-ray diffraction (XRD), scanning electron microscopy (SEM), rheology, mechanical testing, microfluidic transport, electrochemical impedance spectroscopy, chronoamperometry, and smartphone red-green-blue (RGB) analysis were evaluated across six independent batches. APC-CNC-AuPB achieved a limit of detection (LOD) of 0.70 µmol/L, a limit of quantification (LOQ) of 2.34 µmol/L, R^2 of 1.0000, a response time of 26.4 s, a recovery of 101.3%, an intra-batch coefficient of variation (CV) of 0.1%, and 91.6% response retention after 14 days. Deming regression and Bland-Altman analysis showed close agreement with reference glucose concentrations. The platform provided a reproducible artificial sweat framework for optimizing plant-derived hydrogel interfaces before on-body validation.

Keywords: plant polysaccharide hydrogel; sweat glucose; artificial sweat; enzymatic biosensor; microfluidics; dual-mode sensing.

***Corresponding author:** Xiaoqin Xu, Department of Physical Education, Hunan International Economics University, Changsha, Hunan 410205, China. Email: CANDYXU1981@163.com.

Introduction

Exercise changes sweat secretion rate and composition over time, so a skin-interfaced glucose sensor must collect small fluid volumes while maintaining biochemical recognition and stable signal transduction. Integrated perspiration arrays establish that metabolites, electrolytes, and temperature can be monitored during activity [1]. Previous studies on sweat glucose have indicated that low analyte concentrations and the unclear correlation with blood glucose levels are the primary analytical limitations [2]. Optical sweat sensors impose additional requirements regarding illumination, surface chemistry, and portable readout capabilities [3], whereas broader research into wearable sweat sensing focuses on factors such as secretion rate, evaporation, pH, temperature, and skin contaminants [4]. Therefore, post-exercise monitoring is important not because sweat glucose can directly substitute for blood

glucose, but because it enables the tracking of localized, time-varying metabolic patterns under controlled sampling and matrix effect conditions.

Recent platforms have improved the integration of sweat extraction, fluid transport, and glucose measurement. Autonomous extraction systems demonstrate that stimulation, collection, and sensing must be coordinated [5]. Liu *et al*. designed a portable plasmonic nanopillar device that could measure 20 - 600 µmol/L sweat glucose and demonstrated sensitive optical detection with compact instrumentation [6]. Exercise measurement also revealed that sweat glucose differed by anatomical region and time with forehead profiles differing from forearm, scapula, and triceps profiles [7]. These advances define realistic concentration and transport requirements for a post-exercise test platform. However, a remaining issue is that material formulations, microfluidic transport, enzymatic chemical reactions, and signal verification are often evaluated as independent components. Hydrogels may undergo rapid swelling that leads to enzyme leaching, or electrodes may exhibit signal drift in response to fluctuations in sweat rate, pH, or temperature while sensitive in a fixed buffer. Furthermore, comparisons based solely on a single optimized sample make it difficult to elucidate the material properties that determine performance. A useful preclinical platform should therefore compare matched formulations, quantify batch variability, and test both analytical and interfacial properties under controlled artificial sweat conditions. Plant polysaccharides provide hydrated, hydroxyl- and carboxyl-rich networks suitable for enzyme loading [8]. Alginate supports mild ionic gelation and biomedical interfaces [9], and reinforced hydrogel networks can improve resilience without requiring rigid substrates [10]. The egg-box model describes divalent-cation junctions in polyuronates [11], and later work refined this mechanism for alginate and pectin [12]. Pectin chemistry [13], cellulose nanomaterial structure [14], and cellulose nanocrystal self-assembly [15] provide complementary routes to adjust hydration and mechanical order. Recent carboxymethyl cellulose nanocomposite hydrogels [16] and cellulose-paper patches [17] further support plant-derived materials for sweat glucose sensing.

This study constructed and evaluated a plant polysaccharide hydrogel platform for simulated post-exercise sweat glucose detection using alginate colorimetric method as the basis for the design of optical sensing systems [18], while Prussian blue mediator chemistry [19], stable screen-printed enzyme electrodes [20], and the principles of electrochemical glucose biosensors [21] were applied for the design of amperometric detection channels. The microfluidic layout incorporated sweat capture and colorimetric storage concepts [22], integrated electrochemical and volumetric analysis [23], continuous thermoregulatory sweat handling [24], dynamic secretion analysis [25], and low-profile epidermal glucose sensing [26]. Eight formulations were compared by structural, mechanical, microfluidic, electrochemical, colorimetric, and statistical endpoints. This design explored whether a balanced plant-polysaccharide network could provide a reproducible *in vitro* interface for later wearable and human validation.

Materials and methods

Platform design

The platform workflow comprised seven linked operations. Chemically prepared artificial sweat was delivered to a laser-cut elastomeric channel, routed to a plant polysaccharide hydrogel window, exposed to an enzymatic glucose-recognition layer, and measured by electrochemical and colorimetric channels. The resulting signals were converted to glucose concentrations and evaluated by group comparison, regression, agreement, and multivariate analyses. The workflow therefore included fluid delivery, biochemical recognition, signal conversion, and multivariate validation.

Hydrogel formulations and fabrication

The three single-polymer controls contained 1.80% sodium alginate (ALG), citrus pectin (PEC), or sodium carboxymethyl cellulose (CMC) (Aladdin Biochemical Technology Co., Ltd., Shanghai, China). ALG and PEC controls contained 0.32 U/cm² glucose oxidase (GOx) from *Aspergillus niger* (Sigma-Aldrich, St. Louis, MO, USA) and were crosslinked with 80 mM $CaCl_2$. CMC control contained 0.32 U/cm² GOx and 60 mM $CaCl_2$. The dual-polymer formulations were ALG-PEC with 1.20% ALG, 0.60% PEC, 0.40 U/cm² GOx, and 90 mM $CaCl_2$, ALG-CMC with 1.20% ALG, 0.60% CMC, 0.40 U/cm² GOx, and 90 mM $CaCl_2$, and PEC-CMC with 1.00% PEC, 0.80% CMC, 0.40 U/cm² GOx, and 70 mM $CaCl_2$. The ALG-PEC-CMC formulation contained 0.90% ALG, 0.45% PEC, 0.45% CMC, 0.15% cellulose nanocrystals (CNC) (CelluForce, Montreal, QC, Canada), 0.10 mg/mL gold-Prussian blue (AuPB) formed by combining gold nanoparticles (AuNPs) with Prussian blue (Aladdin Biochemical Technology Co., Ltd., Shanghai, China), 0.48 U/cm² GOx, and 100 mM $CaCl_2$. The optimized alginate-pectin-carboxymethyl cellulose (APC)-CNC-AuPB formulation contained the same polysaccharide proportions with 0.30% CNC, 0.25 mg/mL AuPB, 0.55 U/cm² GOx, and 110 mM $CaCl_2$. This composition series enabled direct comparison of polymer network complexity, nanocellulose reinforcement, mediator loading, enzyme loading, and crosslinker concentration. Hydrogels were cast as 600 µm films, ionically crosslinked in the specified $CaCl_2$ solution for 12 min, and equilibrated overnight in phosphate-buffered artificial sweat containing 50 mM sodium chloride, 12 mM potassium chloride, 5 mM urea, 10 mM lactate, 0.2 mM uric acid, 0.1 mM ascorbic acid, and glucose standards from 10 to 700 µmol/L. The artificial sweat reproduced the relative glucose concentration patterns reported for sweat from the forearm, scapula, triceps, and forehead [7]. The method-comparison experiment used 42 independently prepared artificial sweat specimens spanning 18 - 640 µmol/L.

Electrochemical and colorimetric measurements

A C110 screen-printed carbon electrode (Metrohm DropSens, Oviedo, Spain) with a 12.6 mm² circular working area was used. The working electrode received 5 µL of 1.0 mg/mL Prussian-blue suspension and was dried for 30 min at room temperature followed by 5 µL of 2.0 mg/mL AuNP-CNC dispersion for another 30 min of drying. GOx was applied at 0.55 U/cm² in 1.0% w/v BSA containing 0.05% (v/v) glutaraldehyde (Aladdin Biochemical Technology Co., Ltd., Shanghai, China) and incubated at 4°C for 2 hrs. The hydrogel film was then laminated over the active electrode area. Electrochemical measurements were made with a CHI660E workstation (Shanghai Chenhua Instrument Co., Ltd., Shanghai, China). Cyclic voltammetry was recorded from -0.15 to 0.55 V, electrochemical impedance spectroscopy (EIS) from 100 kHz to 0.1 Hz, and chronoamperometry at 0.18 V. Sequential glucose additions were continued until the steady-state current was reached at each calibration concentration. For colorimetry, GOx converted glucose to gluconic acid and hydrogen peroxide. Horseradish peroxidase (HRP) (Sigma-Aldrich, St. Louis, MO, USA) was loaded at 0.50 U/cm² to catalyze the oxidation of 0.40 mmol/L 3,3',5,5'-tetramethylbenzidine (TMB) to produce the blue signal. Each hydrogel window received 50 µL of artificial sweat standard and reacted at 25°C for 5 min. Six independently prepared batches were measured at every glucose concentration. Images were captured with a Huawei P40 smartphone (Huawei Technologies Co., Ltd., Shenzhen, China) in a 5,500 K LED light box at a 15 cm camera-to-sample distance, ISO 100, 1/125 s exposure, and fixed 5,500 K white balance. Mean red-green-blue (RGB) values from the same circular region of interest were extracted with ImageJ 1.54g (National Institutes of Health, Bethesda, MD, USA). The blue/white index was calculated as 255 − (R + G + B)/3 after blank-image normalization.

Microfluidic, structural, and mechanical characterization

The channel was fabricated by cutting a 0.30 mm thick silicone elastomer sheet using a VLS3.60 CO_2 laser (Universal Laser Systems, Scottsdale,

AZ, USA). It measured 20 mm × 1.5 mm × 0.30 mm (length × width × height) and had a calculated internal volume of 9.0 µL. The end of the channel was connected to a hydrogel sensing window with a diameter of 5.0 mm. The channel was bonded to the hydrogel/electrode assembly using 100 µm thick, medical grade, double sided, tape. During the experiments, artificial sweat was injected at flow rates ranging from 0.2 to 4.0 µL/min, and the time required for the fluid to travel from the inlet to the sensing window (i.e., the filling time) was measured. At a glucose concentration of 100 µmol/L, the effects of pH from 4.5 to 7.0 and temperature from 20 to 40°C on the retention of environmental signals were evaluated. Fourier transform infrared (FTIR) was performed using a Nicolet iS50 spectroscopy (Thermo Fisher Scientific, Waltham, MA, USA), and X-ray diffraction (XRD) was done using a D8 Advance modular X-ray powder diffraction system (Bruker, Karlsruhe, Germany). Hydrogels were freeze-dried for scanning electron microscopy (SEM) using Hitachi SU8010 scanning electron microscope (Hitachi High-Tech, Tokyo, Japan) and tested in the hydrated state for wetting and mechanical endpoints. Swelling was calculated from hydrated and dry masses after 30 min of immersion. Contact angle was recorded within 5 s of droplet placement using a DSA100 distributor (KRÜSS, Hamburg, Germany), and pore size was determined from SEM images. Rheological measurements were made with an MCR 302 modular compact rheometer (Anton Paar, Graz, Austria). Tensile, compression, and adhesion tests were conducted using an Instron 5944 tensile and compression tester (Instron, Norwood, MA, USA). Rectangular strips were used for tensile tests and cylindrical punches were used for compression. Adhesion was measured on a gelatin skin model after 2 min under a 5 kPa preload. Self-healing was evaluated after cut-contact recovery, and electrochemical current retention was recorded during 1,000 bending cycles. A 0.1 - 100 Hz rheological frequency sweep measured the storage modulus (G'), which represented the elastic component, and the loss modulus (G"), which represented the viscous component. Conductivity was calculated from impedance spectra and the hydrogel-window geometry.

Statistical analysis

R version 4.3.2 (R Foundation for Statistical Computing, Vienna, Austria) was employed for statistical analysis with lme4 for mixed-effects modelling, emmeans for adjusted comparisons, mcr for Deming regression, BlandAltmanLeh for Bland-Altman analysis, and FactoMineR for principal component analysis. Data were reported as mean ± standard deviation (SD) unless otherwise stated. Each formulation was prepared in six independent batches. Normality and variance homogeneity were evaluated with Shapiro-Wilk and Levene tests. The limit of detection (LOD) and limit of quantification (LOQ) were calculated as 3 and 10 times the blank standard deviation divided by the calibration slope. One-way analysis of variance (ANOVA) with Tukey post hoc comparisons were used to test formulation effects. Holm correction controlled the family-wise error rate for primary endpoints, and false-discovery-rate control was applied to exploratory correlations. Repeated calibrations were evaluated with a batch-level mixed-effects model. Deming regression and Bland-Altman analysis assessed agreement between sensor estimates and reference glucose concentrations. Principal component analysis (PCA) summarized the multivariate formulation profiles. All tests were two-sided, and adjusted *P* value less than 0.05 was considered statistically significant.

Results and discussion

Formulation design and structural characterization

The eight formulations formed a graded series from single polysaccharide controls to the optimized APC-CNC-AuPB network. Single-polymer films were easy to cast but showed either excessive swelling or weak enzyme retention. Dual networks improved hydration and cohesion, whereas the triple network combined alginate and pectin calcium junctions,

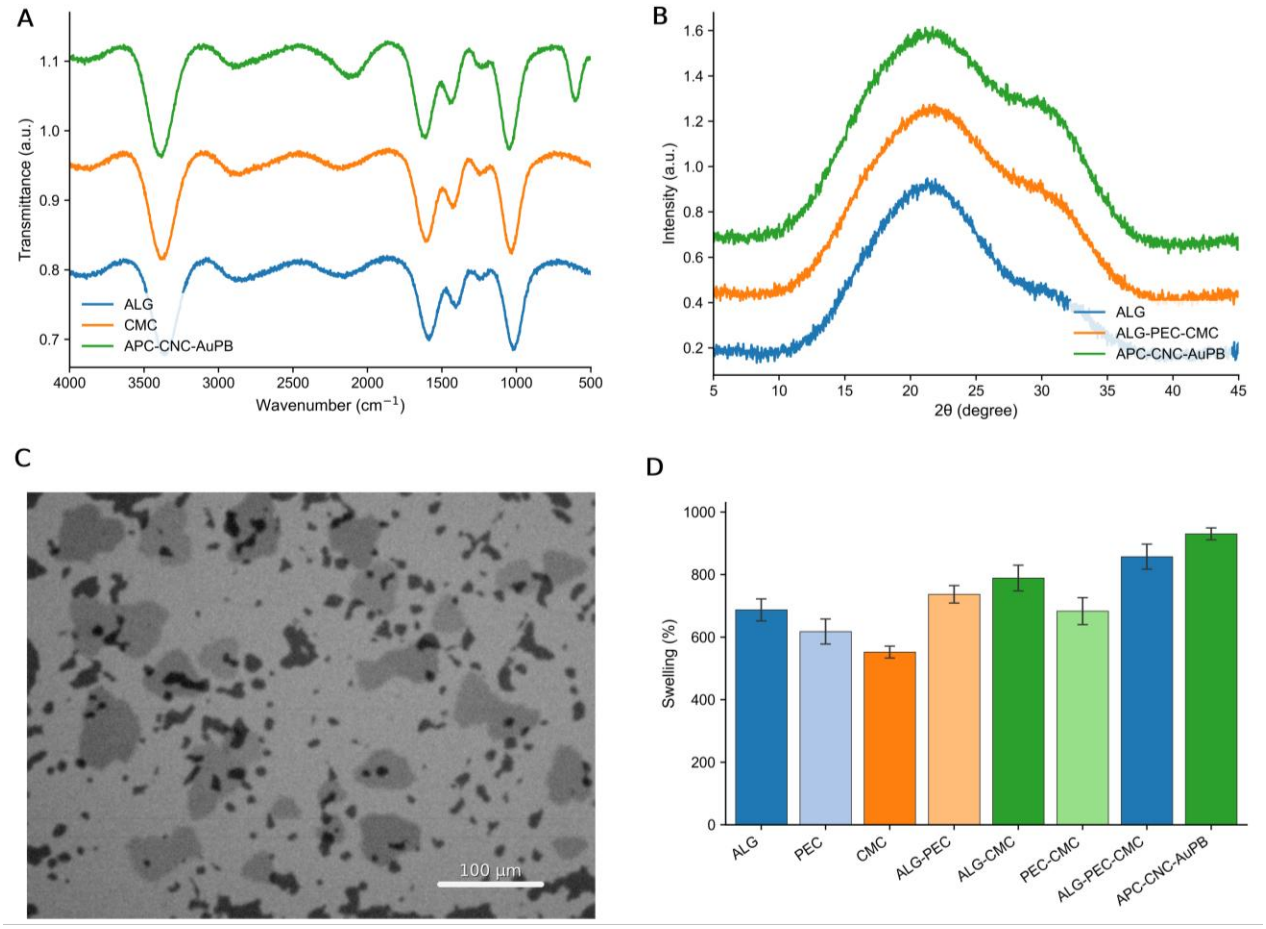


Figure 1. Structural characterization of hydrogel samples. **A.** Fourier transform infrared spectroscopy spectra showing hydroxyl, carboxylate, glycosidic, and low-wavenumber Prussian blue-associated bands. **B.** X-ray diffraction patterns comparing amorphous polysaccharide scattering with cellulose nanocrystal-associated ordered contributions. **C.** Scanning electron microscopy image of the APC-CNC-AuPB porous network. **D.** Swelling ratios for all eight formulations, reported as mean ± standard deviation from six independent batches.

CMC chain entanglement, CNC reinforcement, and AuPB electron-transfer sites. The calcium-mediated junctions were consistent with the egg-box mechanism [11]. CNC provided nanoscale reinforcement [15]. AuPB supplied low-potential mediator sites compatible with screen-printed glucose detection [20]. FTIR and XRD supported formation of the integrated network (Figure 1A, 1B). The hydroxyl band at 3,330 – 3,420/cm remained visible, while the asymmetric carboxylate region near 1,600/cm shifted after Ca^{2+} crosslinking and CNC-AuPB incorporation. The optimized hydrogel also showed a low-wavenumber Prussian blue contribution. XRD retained the broad polysaccharide halo near 21.6 degrees with a secondary contribution near 31 degrees, indicating increased local order without loss of the hydrated amorphous matrix. SEM demonstrated an interconnected porous APC-CNC-AuPB network with a target pore size of 38 µm (Figure 1C). The optimized hydrogel reached 930 ± 19% swelling compared with 687 ± 35% for ALG (Figure 1D) with contact angle of 23.8 ± 0.4 degrees, indicating faster initial wetting than the control films. This behavior was consistent with hydroxyl- and carboxyl-rich plant polysaccharide gels [8].

Mechanical, rheological, and interfacial performance

The tensile curves increased monotonically over the tested strain range. APC-CNC-AuPB sustained

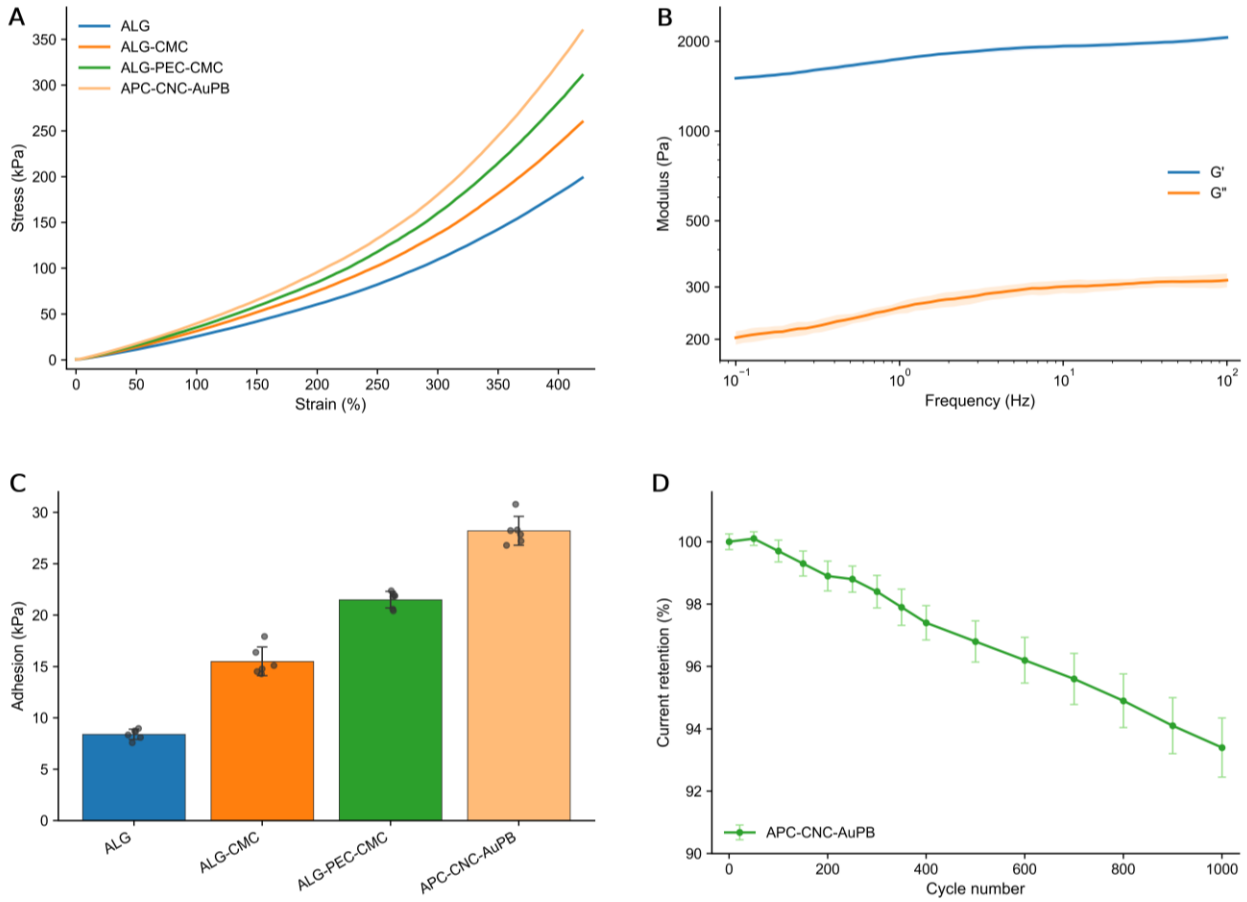


Figure 2. Mechanical and interfacial performance. **A.** Tensile stress-strain response of representative ALG, ALG-CMC, ALG-PEC-CMC, and APC-CNC-AuPB films. **B.** Rheological frequency sweep showing storage modulus (G′) and loss modulus (G″) across 0.1 - 100 Hz. **C.** Adhesion to a gelatin skin model reported as mean ± standard deviation. **D.** Electrochemical current retention during 1,000 bending cycles.

Table 1. Physical, mechanical, and interfacial properties of hydrogel samples in 6 independent batches.

Sample	Swelling (%)	Contact angle (degree)	Modulus (kPa)	Toughness (MJ/m³)	Adhesion (kPa)	Self-healing (%)
ALG	687 ± 35	58.3 ± 3.5	36.2 ± 2.1	1.10 ± 0.08	8.4 ± 0.5	60.0 ± 1.4
ALG-CMC	789 ± 41	36.4 ± 2.6	62.6 ± 4.1	2.14 ± 0.14	15.5 ± 1.4	78.3 ± 2.3
ALG-PEC	737 ± 28	42.9 ± 2.1	60.0 ± 1.4	1.84 ± 0.12	13.6 ± 1.1	74.6 ± 1.6
ALG-PEC-CMC	857 ± 40	30.7 ± 2.7	82.3 ± 5.1	2.91 ± 0.12	21.5 ± 0.8	86.9 ± 2.4
APC-CNC-AuPB	930 ± 19	23.8 ± 0.4	107.6 ± 8.4	3.77 ± 0.27	28.2 ± 1.4	93.1 ± 4.1
CMC	552 ± 19	50.4 ± 1.4	42.6 ± 3.0	1.30 ± 0.13	9.9 ± 0.5	66.0 ± 2.3
PEC	618 ± 40	62.9 ± 2.3	27.1 ± 1.0	0.83 ± 0.06	7.7 ± 0.7	57.8 ± 1.9
PEC-CMC	683 ± 43	42.4 ± 1.4	53.1 ± 1.1	1.75 ± 0.12	14.6 ± 1.0	73.9 ± 2.9

the highest stress at matched strain without early brittle failure (Figure 2A). The swelling, contact angle, modulus, toughness, adhesion, and self-healing demonstrated that the compressive modulus increased from 36.2 ± 2.1 kPa for ALG to 107.6 ± 8.4 kPa for APC-CNC-AuPB. The formulation effect was significant with $F = 251.3$, Holm-adjusted $P < 0.001$, and $\eta^2 = 0.98$. The optimized film could be laminated and peeled without tearing. The storage modulus G′

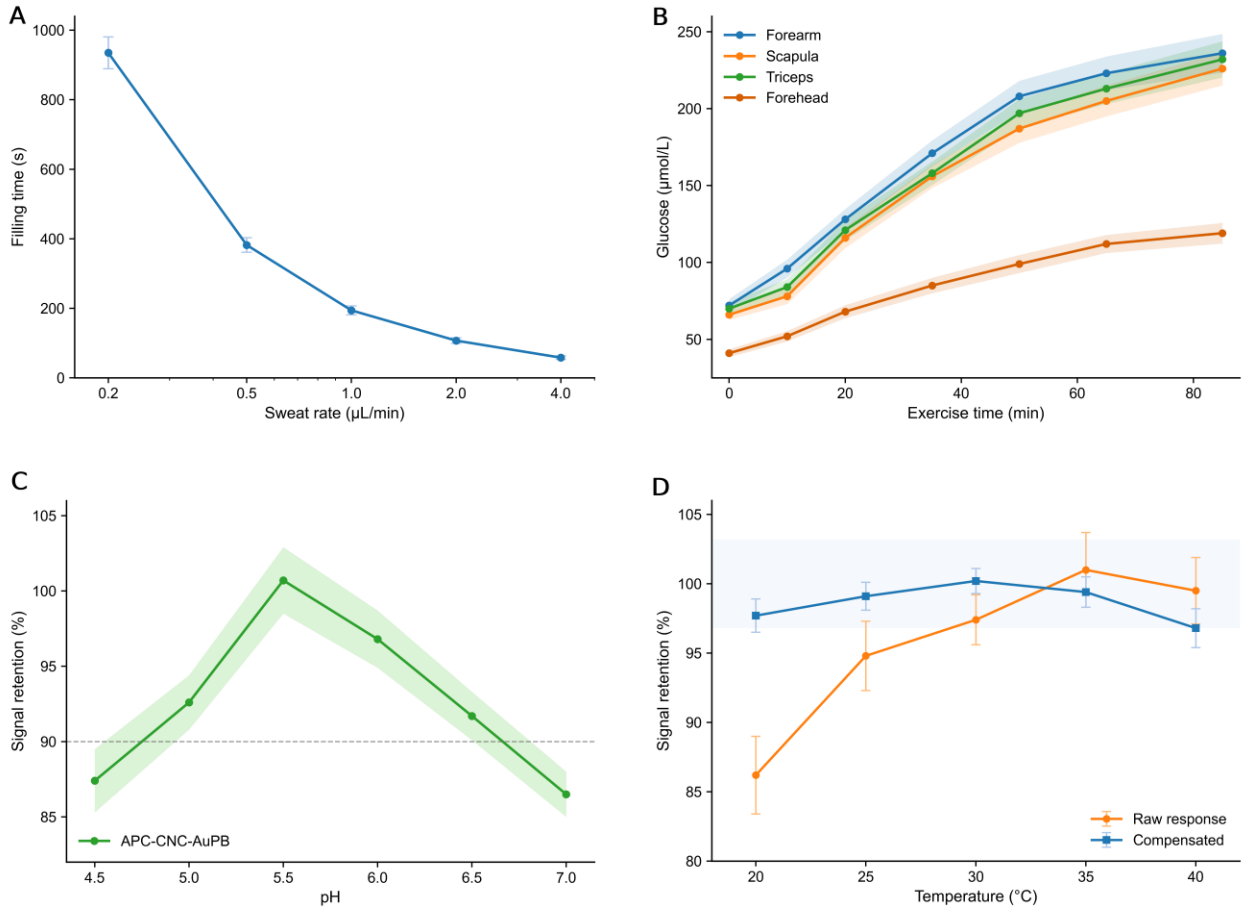


Figure 3. Microfluidic and environmental performance. **A.** Channel filling time across artificial sweat flow rates of 0.2 - 4.0 µL/min. **B.** Programmed artificial sweat glucose profiles representing literature-informed forearm, scapula, triceps, and forehead patterns. **C.** pH robustness at 100 µmol/L glucose. **D.** Raw and compensated temperature responded across 20 - 40°C.

exceeded the loss modulus G" across 0.1 - 100 Hz, confirming elastic dominance under small oscillatory strain (Figure 2B). Adhesion to the gelatin skin model reached 28.2 ± 1.4 kPa for APC-CNC-AuPB and 8.4 ± 0.5 kPa for ALG (Figure 2C). The formulation effect was significant with $F = 301.9$, Holm-adjusted $P < 0.001$, and $\eta^2 = 0.98$. Self-healing reached 93.1 ± 4.1%, and the electrochemical signal retained 93.4% after 1,000 bending cycles (Figure 2D) (Table 1).

Microfluidic transport and environmental robustness

The results showed that increasing artificial sweat flow from 0.2 to 4.0 µL/min shortened channel filling time from approximately 935 to 58 s (Figure 3A). At 1.0 - 4.0 µL/min, fluid reached the hydrogel window within the time scale required for post-exercise sampling. This result supported the use of an integrated skin-interfaced channel in which fluid handling and biochemical readout were evaluated together [23]. The programmed regional profiles were generated with artificial sweat glucose standards and did not use human sweat (Figure 3B). Forearm, scapula, and triceps programs increased from approximately 66 - 72 µmol/L at 0 min to 219 - 236 µmol/L at 85 min, whereas the forehead program increased from 41 to 119 µmol/L. These input profiles reproduced the relative regional and temporal patterns reported during exercise [7], confirmed that the 10 - 700 µmol/L calibration interval covered all programmed values. At 100 µmol/L glucose, signal retention remained above 91% from pH 5.0 to 6.5 and above 86% across pH 4.5 - 7.0 (Figure

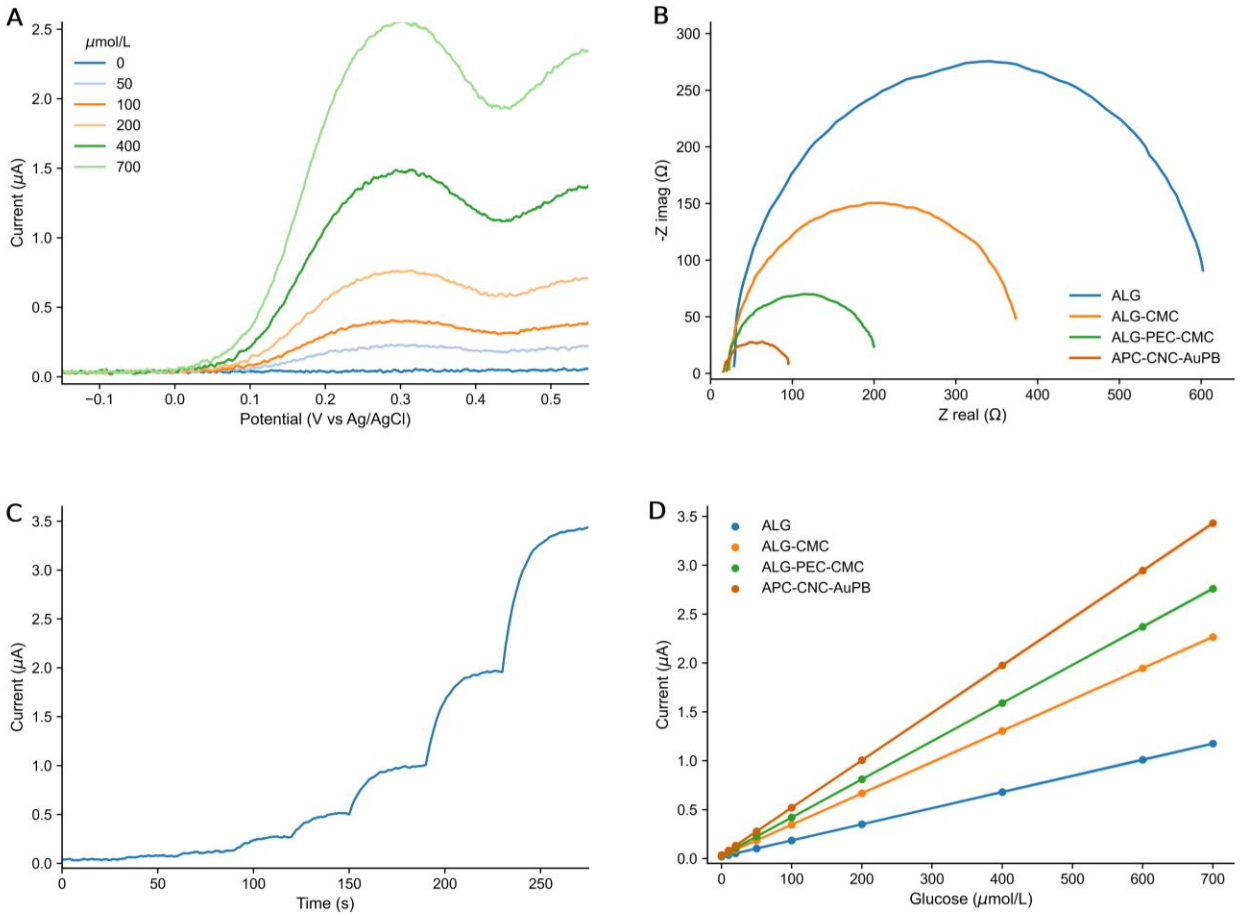


Figure 4. Electrochemical glucose detection. **A.** Cyclic voltammetry at increasing glucose concentrations. **B.** Electrochemical impedance spectroscopy Nyquist plots comparing charge-transfer behavior. **C.** Chronoamperometric staircase response to sequential glucose additions. **D.** calibration curves for representative formulations with 95% confidence intervals.

3C). Temperature changed the raw response more strongly, but compensation reduced residual error to 3.2% across 20 - 40 °C (Figure 3D). The results showed that flow, pH, and temperature needed to be included in platform validation rather than treated as fixed background conditions.

Electrochemical detection performance

Cyclic voltammetry produced concentration-dependent current increases (Figure 4A), while EIS showed progressively lower charge-transfer resistance in CNC-AuPB-containing hydrogels (Figure 4B). APC-CNC-AuPB reached a conductivity of 2.32 ± 0.22 mS/cm, nearly one order of magnitude higher than ALG. The formulation effect was significant with F = 364.6, Holm-adjusted $P < 0.001$, and $\eta^2 = 0.98$. The improvement was consistent with Prussian blue-mediated peroxide detection in screen-printed electrodes [20]. The chronoamperometric staircase stabilized after each glucose addition (Figure 4C), and calibration slopes increased with network complexity (Figure 4D). Across all eight formulations, the LOD ranged from 0.70 to 5.72 µmol/L, the LOQ from 2.34 to 19.08 µmol/L, response time from 26.4 to 60.1 s, recovery from 90.8% to 101.3%, and day-14 retention from 57.2% to 91.6%. APC-CNC-AuPB had the highest slope of 0.00485 µA per µmol/L, the lowest LOD of 0.70 µmol/L, an LOQ of 2.34 µmol/L, and R^2 = 1.0000 over 10 - 700 µmol/L. APC-CNC-AuPB

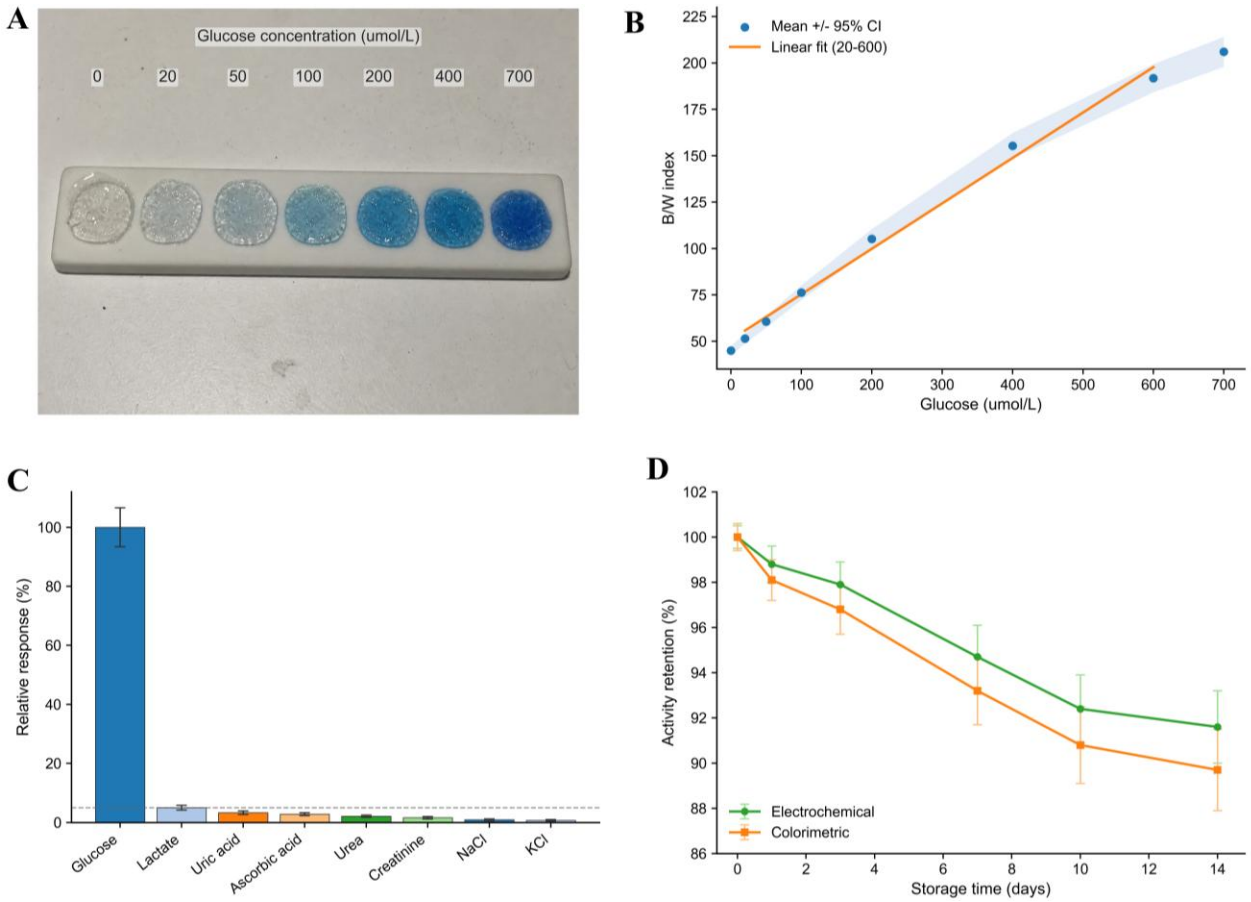


Figure 5. Colorimetric response, selectivity, and stability. **A.** Smartphone color field generated by the glucose oxidase/horseradish peroxidase/3,3′,5,5′-tetramethylbenzidine reaction from 0 to 700 µmol/L glucose. **B.** Red-green-blue-derived blue/white calibration. **C.** Relative responses to glucose and common artificial sweat interferents. **D.** 14-day storage stability of APC-CNC-AuPB at 4°C.

reached 95% of steady signal in 26.4 ± 1.1 s, whereas ALG required 52.8 ± 3.6 s. The formulation effect was significant with F = 139.6, Holm-adjusted $P < 0.001$, and $\eta^2 = 0.96$. The batch-level mixed-effects model produced a glucose slope of 0.00485 µA per µmol/L ($P < 0.001$) with low random batch variance, indicating that calibration was driven by concentration rather than one atypical film.

Colorimetric response, selectivity, and storage stability

The GOx/HRP/TMB reaction produced a concentration-dependent blue field from 0 to 700 µmol/L glucose (Figure 5A). The RGB-derived blue/white calibration remained useful from 20 to 700 µmol/L, although optical saturation compressed the response above 600 µmol/L (Figure 5B). The optimized hydrogel had a colorimetric LOD of 3.6 µmol/L, which was consistent with alginate-based colorimetric sweat glucose detection [18]. The selectivity was tested against common artificial sweat components with glucose at 100 µmol/L as 100%. The results showed that lactate at 10 mM produced 5.0%, while uric acid, ascorbic acid, urea, creatinine, NaCl, and KCl each produced less than 5% of the glucose response (Figure 5C). The low working potential of the Prussian blue mediator limited oxidation of electroactive interferents [19]. Storage stability was assessed and demonstrated that, after 14 days at 4°C, APC-CNC-AuPB retained 91.6% of the electrochemical response and 89.7% of the colorimetric response, whereas ALG and PEC retained approximately 60 - 62%. APC-CNC-AuPB recovered 101.3 ± 2.6% of

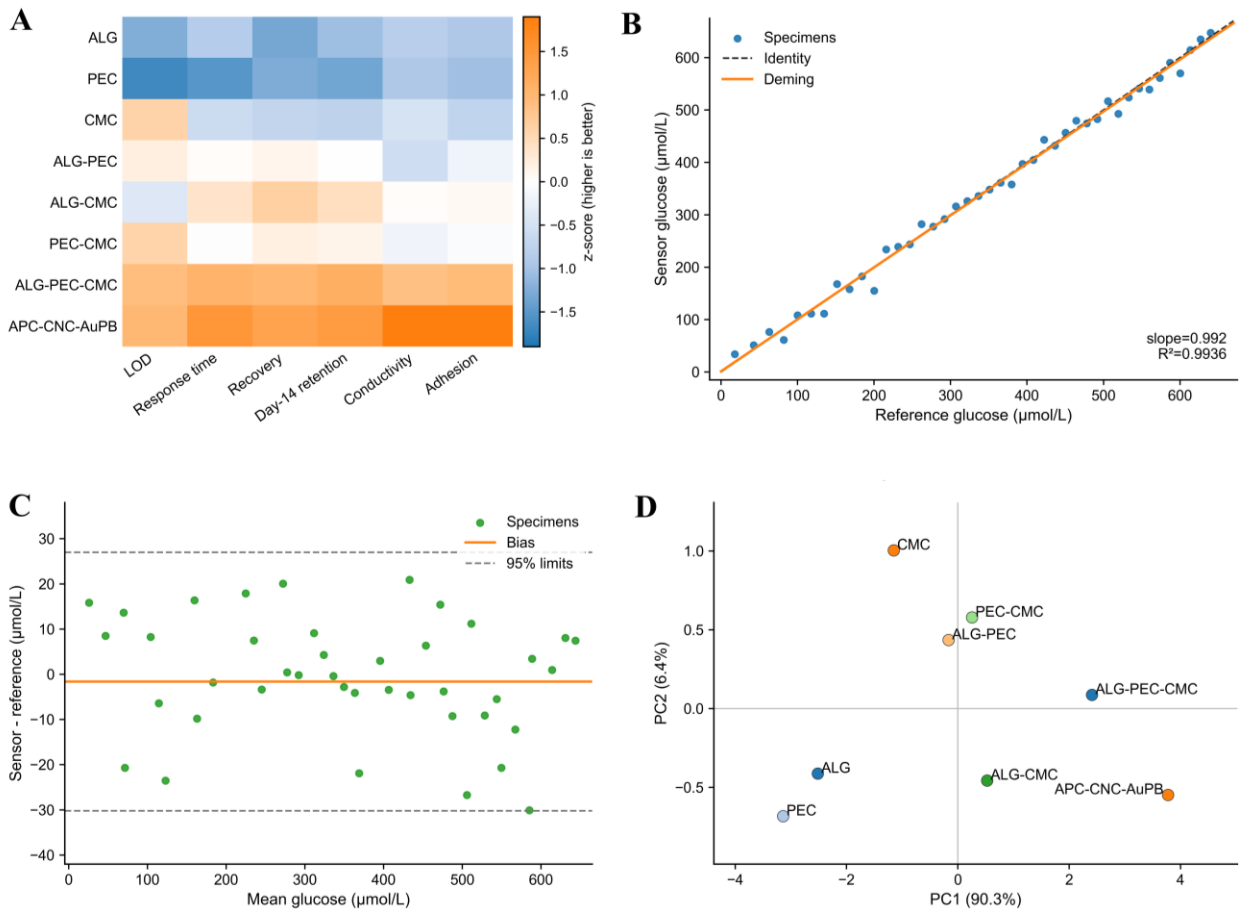


Figure 6. Integrated statistical evaluation. **A.** Normalized z-score heatmap comparing limit of detection, response time, recovery, 14-day retention, conductivity, and adhesion. **B.** Deming regression of electrochemical estimates against reference glucose concentrations. **C.** Bland-Altman plot showing bias and 95% limits of agreement. **D.** Principal component analysis of platform metrics.

spiked glucose and had intra- and inter-batch CVs of 0.1% and 0.2%, respectively (Figure 5D).

Integrated statistical evaluation, implications, and limitations

The normalized performance heatmap compared all formulations across LOD, response time, recovery, day-14 retention, conductivity, and adhesion. APC-CNC-AuPB occupied the most balanced high-performance region with no single material endpoint that alone reproduced this ranking (Figure 6A). The agreement analysis showed that Deming regression gave a slope of 0.992, an intercept of 1.2 µmol/L, and $R^2 = 0.9939$ for 42 artificial sweat specimens (Figure 6B). Bland-Altman analysis showed a mean bias of -1.6 µmol/L and 95% limits of agreement from -30.2 to 27.0 µmol/L (Figure 6C). The mean absolute relative difference was 7.1%. The principal component analysis separated the optimized sample from single-network controls mainly along analytical sensitivity and interface-stability dimensions (Figure 6D). Assumption checks supported parametric comparison of the primary endpoints. The minimum Shapiro-Wilk *P* value for batch-level modulus distributions exceeded 0.05, and Levene testing did not show severe variance heterogeneity for modulus. Conductivity, response time, adhesion, and LOD showed the largest standardized formulation effects. These results linked the CMC/CNC/AuPB architecture to measurable changes in electron transfer, wetting, mechanics, and analytical response. However, the *in vitro* design defined the study's limitations. Artificial sweat did not reproduce proteins, skin lipids, cosmetics,

microbial products, or dynamic evaporation on the skin. The programmed regional profiles demonstrated the platform's response to literature-informed concentration patterns but could not support physiological inference. Enzyme-based devices also remained sensitive to long-term humidity and temperature excursions. Future work should therefore include paired on-body sweat measurements, perspiration rate normalization, wireless electronics, and subject level calibration. The results of this study suggested that a plant polysaccharide hydrogel could function as an active, adhesive, enzyme-retaining, and microfluidically coupled sensing interface. APC-CNC-AuPB combined an LOD below 1 µmol/L, recovery near 100%, response below 30 s, and more than 90% day-14 retention. The platform therefore provided a controlled material and analytical foundation for subsequent wearable validation.

Acknowledgements

This work was supported by the General Project of Humanities and Social Sciences Research of the Ministry of Education (Grant No. 24YJA890039), the Hunan Provincial Philosophy and Social Sciences Foundation (Grant No. 21YBA220), and the Hunan Province New Liberal Arts Research and Practice Project (Xiangjiaotong [2025] No. 131 [109]).

References

1. Gao W, Emaminejad S, Nyein HYY, Challa S, Chen K, Peck A, *et al*. 2016. Fully integrated wearable sensor arrays for multiplexed *in situ* perspiration analysis. Nature. 529(7587):509-514.
2. Zafar H, Channa A, Jeoti V, Stojanović GM. 2022. Comprehensive review on wearable sweat-glucose sensors for continuous glucose monitoring. Sensors (Basel). 22(2):638.
3. Wang J, Luo Y, Zhou Z, Xiao J, Xu T, Zhang X. 2024. Epidermal wearable optical sensors for sweat monitoring. Commun Mater. 5(1):77.
4. Bariya M, Nyein HYY, Javey A. 2018. Wearable sweat sensors. Nat Electron. 1(3):160-171.
5. Emaminejad S, Gao W, Wu E, Davies ZA, Nyein HYY, Challa S, *et al*. 2017. Autonomous sweat extraction and analysis applied to cystic fibrosis and glucose monitoring using a fully integrated wearable platform. Proc Natl Acad Sci USA. 114(18):4625-4630.
6. Liu L, Zhan K, Kilpijärvi J, Kinnunen M, Zhao Y, Zhang Y, *et al*. 2026. Portable and label-free optical detection of sweat glucose using functionalized plasmonic nanopillar array. Microsyst Nanoeng. 12(1):43.
7. King MA, Brown SD, Barnes KA, De Chavez PJD, Baker LB. 2023. Regional and time course differences in sweat cortisol, glucose, and select cytokine concentrations during exercise. Eur J Appl Physiol. 123(8):1727-1738.
8. Bahú JO, de Andrade LRM, de Melo Barbosa R, Crivellin S, da Silva AP, Souza SDA, *et al*. 2022. Plant polysaccharides in engineered pharmaceutical gels. Bioengineering (Basel). 9(8):376.
9. Lee KY, Mooney DJ. 2012. Alginate: properties and biomedical applications. Prog Polym Sci. 37(1):106-126.
10. Sun JY, Zhao X, Illeperuma WR, Chaudhuri O, Oh KH, Mooney DJ, *et al*. 2012. Highly stretchable and tough hydrogels. Nature. 489(7414):133-136.
11. Grant GT, Morris ER, Rees DA, Smith PJC, Thom D. 1973. Biological interactions between polysaccharides and divalent cations: The egg-box model. FEBS Lett. 32(1):195-198.
12. Braccini I, Pérez S. 2001. Molecular basis of Ca^{2+}-induced gelation in alginates and pectins: The egg-box model revisited. Biomacromolecules. 2(4):1089-1096.
13. Mohnen D. 2008. Pectin structure and biosynthesis. Curr Opin Plant Biol. 11(3):266-277.
14. Moon RJ, Martini A, Nairn J, Simonsen J, Youngblood J. 2011. Cellulose nanomaterials review: Structure, properties and nanocomposites. Chem Soc Rev. 40(7):3941.
15. Habibi Y, Lucia LA, Rojas OJ. 2010. Cellulose nanocrystals: Chemistry, self-assembly, and applications. Chem Rev. 110(6):3479-3500.
16. Zhou T, Liu J, Liu P, Wang W, Bai L, Chen H, *et al*. 2024. Carboxymethyl cellulose sodium nanocomposite hydrogels for flexible sensors of human motion and glucose levels in sweat. ACS Appl Polym Mater. 6(13):7393-7407.
17. Karim Z, Khan MJ, Hussain A, Ahmed F, Khan ZH. 2024. Multilayer patch functionalized microfibrillated cellulosic paper sensor for sweat glucose monitoring. Sci Rep. 14(1):23434.
18. Garcia-Rey S, Gil-Hernandez E, Basabe-Desmonts L, Benito-Lopez F. 2023. Colorimetric determination of glucose in sweat using an alginate-based biosystem. Polymers (Basel). 15(5):1218.
19. Ricci F, Palleschi G. 2005. Sensor and biosensor preparation, optimisation and applications of Prussian Blue modified electrodes. Biosens Bioelectron. 21(3):389-407.
20. Ricci F, Amine A, Tuta CS, Ciucu AA, Lucarelli F, Palleschi G, *et al*. 2003. Prussian Blue and enzyme bulk-modified screen-printed electrodes for hydrogen peroxide and glucose determination with improved storage and operational stability. Anal Chim Acta. 485(1):111-120.
21. Wang J. 2008. Electrochemical glucose biosensors. Chem Rev. 108(2):814-825.
22. Koh A, Kang D, Xue Y, Lee S, Pielak RM, Kim J, *et al*. 2016. A soft, wearable microfluidic device for the capture, storage, and colorimetric sensing of sweat. Sci Transl Med. 8(366):366ra165.

23. Bandodkar AJ, Gutruf P, Choi J, Lee K, Sekine Y, Reeder JT, *et al*. 2019. Battery-free, skin-interfaced microfluidic/electronic systems for simultaneous electrochemical, colorimetric, and volumetric analysis of sweat. Sci Adv. 5(1):eaav3294.
24. Nyein HYY, Bariya M, Tran B, Ahn CH, Brown BJ, Ji W, *et al*. 2021. A wearable patch for continuous analysis of thermoregulatory sweat at rest. Nat Commun. 12(1):1823.
25. Nyein HYY, Tai LC, Ngo QP, Chao M, Zhang GB, Gao W, *et al*. 2018. A wearable microfluidic sensing patch for dynamic sweat secretion analysis. ACS Sens. 3(5):944-952.
26. Bandodkar AJ, Jia W, Yardımcı C, Wang X, Ramirez J, Wang J. 2015. Tattoo-based noninvasive glucose monitoring: A proof-of-concept study. Anal Chem. 87(1):394-398.